EUROTeV-Report-2006-094
Cockcroft-06-84

Vacuum Systems for the ILC Damping Rings

Oleg B. Malyshev[1,2]

November 24, 2006

Abstract

Damping rings are important subsystems of the International Linear Collider (ILC). In this paper, we consider the vacuum specifications that and consider possible vacuum system design solutions for these rings. Our aim is to find the optimum approach to the vacuum system technology in order to achieve the required vacuum levels with reasonable conditioning time. It turns out that the optimum vacuum design uses a NEG coated tubular vacuum chamber. In this case, since almost all inner surface of vacuum chamber will be NEG coated, the gas density along the beam does not depend on the choice of material for a vacuum chamber. The choice of vacuum chamber material between stainless steel, aluminium and copper is then driven by beam impedance, thermal conductivity requirement and cost.

[1] ASTeC, Daresbury Laboratory, Warrington, WA44AD,England
[2] Cockcroft Institute, Warrington, WA4 4AD,England

1. Introduction

The damping rings (DR) of the International Linear Collider (ILC) will provide high quality electron and positron beams for achieving the required luminosity at the interaction point. The vacuum system is one of the key components in the ILC damping rings. In the present baseline configuration [1], the total length of beam vacuum chamber is about 20 km. The OCS design suggests 6 km damping rings: one electron ring and two positron rings. Having two positron rings helps to avoid significant electron cloud build up and electron multipacting in the beam vacuum chamber.

Modern vacuum technology can provide a wide variety of means for reaching the required gas density along the beam trajectory. There are a number of similarities in the vacuum design of the damping rings and storage rings for synchrotron radiation sources: there are well-known vacuum problems, such as thermal and photon induced gas desorption, and there are several conventional methods of dealing with them. Meanwhile there are important differences such as electron multipacting and electron cloud build-up, ion cloud build-up (ion instability), and ion induced pressure instability. The choice of optimum vacuum technology requires study of all these effects. Where these effects play a dominant role, conventional technology may not be applicable and some dedicated experimental and theoretical research is required.

Effects that can significantly impact the damping ring vacuum include:

- thermal stimulated desorption (which limits the pressure in the long straight);
- photon stimulated desorption (in the arcs, wigglers, short straights);
- electron stimulated desorption due to beam-induced electron multipacting in the positron ring;
- ion stimulated desorption from ionisation of the residual gas particles, which are then accelerated toward the vacuum chamber walls by the beam in the positron ring.

The need to avoid fast ion instability leads to very demanding specifications for the vacuum in the electron damping ring: < 0.5 nTorr CO in the arc cell, < 2 nTorr CO in the wiggler cell and < 0.1 nTorr CO in the straight section [2].

In this paper the effect of thermal and photon stimulated desorption is studied. The effect of electron multipacting will be studied in future if there is a change in the configuration to have one positron DR only, which may led to higher das desorption due to multipacting electrons.

2. Sources of Gas in a Vacuum System

To perform a vacuum design for the damping rings, the sources of gas should be identified first.

2.1. Thermal stimulated desorption

Most materials placed in a vacuum desorb molecules of gas, and are therefore sources of gas in a vacuum chamber. The desorption rate depends on the material, its cleaning, treatment, pre-history and many other factors. The thermal desorption rate for stainless steel, well-known as a good vacuum material, can be reduced to the level of 10^{-12} Torr·l/(s·cm^2) for CO after 24 hrs bake-out at 300ºC and weeks of pumping.

2.2. Photon stimulated desorption

Synchrotron radiation generated by the electron or positron beam in dipoles and wigglers will irradiate the vacuum chamber walls. Even in the case of an antechamber with lumped SR absorbers, some non-negligible fraction of photons generated by the undulator will irradiate the walls of the vacuum chamber. Photon interactions with a surface cause photoelectron emission; emitted electrons have a certain probability to desorb gas molecules from the surface both in the place where they are emitted, and where they collide with a surface.

Synchrotron radiation from other magnetic elements (quadrupoles and sextupoles) is here regarded as negligible, since the beam should go along the magnetic axes of these elements where the field strength is zero; were the beams offset from the axis, then SR from these elements would have to be considered.

2.2.1. PSD yield as a function of photon dose

Photodesorption yields, η (molecules/photon), depend on the material, cleaning, treatment, pre-history and accumulated photon dose. There are several experimental results published in literature for photodesorption yields, η, measured as a function of accumulated photon dose, D, for different materials and measured up to certain photon doses (for example, see [3,4,5]). Schematically, a typical behaviour of the desorption yield as a function of photon dose is shown in Figure 1. Initially, the photodesorption yield might be almost independent (for instance, stainless steel after bakeout at 300°C for 24 hrs with doses up to ~10^{21} photons/m) or have very low dependence on photon dose (as copper and aluminium); then, for larger irradiation time, the photodesorption yield at room temperature can be described as a function of accumulated photon dose as:

$$h = h_0 \left(\frac{D_0}{D} \right)^a, \quad 0.65 < a < 1$$

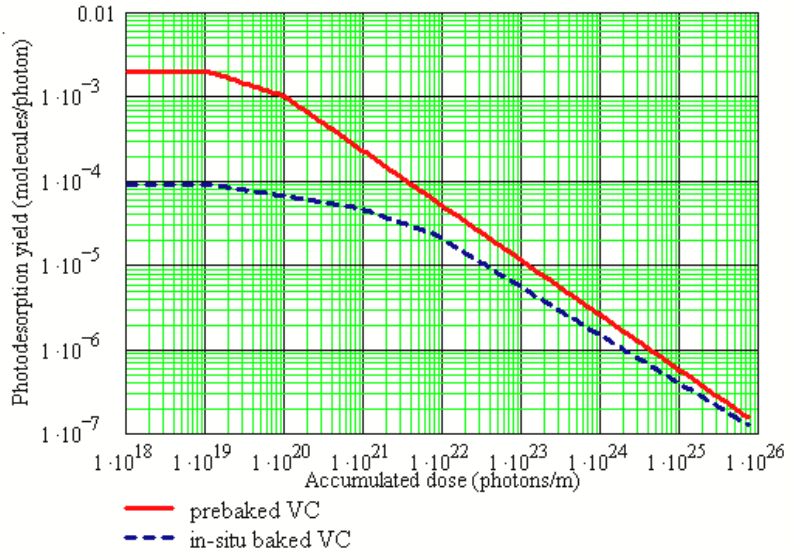

Figure 1. PSD yield for CO for pre-baked and in-situ baked stainless steel vacuum chambers. Yields for doses higher then 10^{23} photons/m (1 to 10 Amp×hrs for diamond) are extrapolations.

2.2.2. PSD yield as a function of photon critical energy

The photon desorption also depends on photon energy. There have been several studies that have shown that the photon stimulated desorption yield grows with photon critical energy as follows:

- proportional to the critical photon energy ε_c when $\varepsilon_c < 1$ keV [6];
- weak increase with the critical photon energy ε_c when 1 keV < ε_c < 100 keV [6,7];
- proportional to either the critical photon energy ε_c or to the SR power when ε_c > 100 keV [7].

This means that data received in photodesorption experiments, measured at a few keV photon critical energy are directly applicable to the damping ring.

2.3. Gas dynamic model

Consider a simple vacuum chamber consisting of a circular tube with inner diameter *d* and a length *L* between two pumps with an effective pumping speed *S*. The tube has a vacuum conductance *u* and, if it is NEG coated, may pump with a sticking probability a.

The general equations of gas dynamic balance inside a vacuum chamber with sorbing walls can be written as [8]:

$$V\frac{dn}{dt} = h\dot{\Gamma} - aCn + u\frac{d^2n}{dz^2}; \qquad (1)$$

where n *[molecules/cm^3]* is the volume gas density;
V *[cm^3]* is the vacuum chamber volume;
A *[cm^2]* is the vacuum chamber wall area;
h *[molecules/photon]* is the primary photodesorption yield;
$\dot{\Gamma}$ *[photon/(sec·cm)]* is the photon intensity per unit axial length;
a is the sticking probability;
$C = A\bar{v}/4$ is the ideal wall pumping speed, $\bar{v}$ is the mean molecular velosity;
n_e *[molecules/cm^3]* is the thermal equilibrium gas density;
$u = A_c D$ is the specific vacuum chamber conductance per unit axial length, A_c is the vacuum chamber cross section; D is the Knudsen diffusion coefficient.

In the quasi-static conditions with $V\frac{\partial n}{\partial t} \approx 0$ the gas density is described by a second order differential equation for $n(z)$:

$$u\frac{d^2n}{dz^2} - aCn + h\dot{\Gamma} = 0. \qquad (2)$$

The second order differential equation (2) for the function $n(z)$ has two solutions:

Case (a)
$$n(z) = \frac{h\dot{\Gamma}}{aC} + C_1 e^{\sqrt{\frac{aC}{u}}z} + C_2 e^{-\sqrt{\frac{aC}{u}}z} \quad \text{for } c > 0 \qquad (3)$$

Case (b)
$$n(z) = -\frac{h\dot{\Gamma}}{2u}z^2 + C_5 z + C_6 \qquad \text{for } c = 0 \qquad (4)$$

where the constants depend on the boundary conditions.

In order to study the evolution of the gas density within an accelerator vacuum chamber, the simplest case of an infinitely long tube is studied in the following section. Subsequently, the conditions at the ends of the chamber are taken into account and their influence on the gas density analysed.

2.3.1. Solution for a short vacuum chamber with a given pressure at the ends

This case can be used both for the case of operation of the accelerator, and in the case of a laboratory experiment. Consider a vacuum chamber centered at $z = 0$, of length L, and with gas density at the ends of $n(-L/2) = n_1$ and $n(L/2) = n_2$. As discussed previously, there are two different solutions for the gas density, depending on the value of the parameter c, given by (3)–(4):

Case (a): sorbing walls, $c > 0$

$$C_1 = \frac{n_1 + n_2 - 2n_{\text{inf}}}{4\cosh\left(\frac{wL}{2}\right)} + \frac{n_2 - n_1}{4\sinh\left(\frac{wL}{2}\right)}; \quad C_2 = \frac{n_1 + n_2 - 2n_{\text{inf}}}{4\cosh\left(\frac{wL}{2}\right)} + \frac{n_1 - n_2}{4\sinh\left(\frac{wL}{2}\right)}.$$

For $n_1 = n_2$ the expression for the gas density may be written as

$$n(z) = n_{\text{inf}} - (n_{\text{inf}} - n_1)\frac{\cosh(wz)}{\cosh\left(\frac{wL}{2}\right)}; \tag{5}$$

where $n_{\text{inf}} = \frac{h\dot{\Gamma}}{aC}$ and $w = \sqrt{aC/u}$.

Case (b): non-sorbing walls, $c = 0$

The expression for the gas density is:

$$n(z) = \frac{h\dot{\Gamma}}{2u}\left(\left(\frac{L}{2}\right)^2 - z^2\right) + \frac{n_1 - n_2}{2L}z + \frac{n_1 + n_2}{2}. \tag{6}$$

This solution is always stable and corresponds to a parabolic pressure profile.

2.3.2. Solution for a short vacuum chamber with a given pumping speed at the ends

Consider a vacuum chamber of length L centered at $z = 0$, with pumps at the two ends of pumping speed S. The conditions at the ends are:

$$n(\pm L/2) = \mp\frac{dn(\pm L/2)}{dz}\frac{u}{S}.$$

In **case (a)** when $c > 0$ the gas density $n(z)$ is given by:

$$n(z) = n_{\text{inf}}\left(1 - \frac{\cosh(wz)}{\cosh\left(\frac{wL}{2}\right)\left(1 + \frac{u}{S}w\tanh\left(\frac{wL}{2}\right)\right)}\right). \tag{7}$$

It is useful to calculate the average value of the gas density in the vacuum chamber of length L:

$$\langle n(L)\rangle = n_{\inf}\left(1-\frac{2\tanh\left(\frac{wL}{2}\right)}{\frac{wL}{2}\left(1+\frac{u}{S}w\tanh\left(\frac{wL}{2}\right)\right)}\right). \quad \textbf{(8)}$$

In **case (b)** when $c=0$ the gas density *n(z)* is given by:

$$n(z) = h\dot{\Gamma}\left[\frac{1}{2u}\left(\left(\frac{L}{2}\right)^2 - z^2\right)+\frac{L}{2S}\right]. \quad \textbf{(9)}$$

The average value of the gas density in the vacuum chamber of length L in this case is:

$$\langle n(L)\rangle = h\dot{\Gamma}\left(\frac{L}{12u}+\frac{1}{2S}\right)L\,. \quad \textbf{(10)}$$

3. Calculations of flux and energy of photons irradiating the damping ring walls

The parameters we used for modelling the gas density along the damping ring are shown in

Table 1.

For purposes of vacuum analysis, the damping ring consists of 6 m or 3 m long dipoles where SR is generated, and straight sections of varying length where no SR is generated. There are many short straights of 32.9, 43.8 or 58.7 m long and two long straights 404.6 m long. There are also eight wiggler sections, each with five wigglers of length 6.3 m located sequentially (31.5 m total section length) where SR is generated within short straights of length 43.8 m.

Assuming a circular vacuum chamber with ID 50 mm in the dipoles and straights, and the dipole vacuum chamber bending with the bending radius of the dipole magnet, the photon flux inside and downstream of the dipole was calculated as a function of distance from the dipole. The results are shown in Figure 2 and Figure 3.

The photon reflectivity from the vacuum chamber walls may be considered as well, but the impact on gas desorption will be insignificant since forward scattered photons are mainly low energy and have lower desorption yield than direct photons.

Table 1. DR & Beam Parameters

	Arc cell	Wiggler cell	Straight section
Number of dipole/wiggler cells per beamline (ring)	120	40	—
Sectorisation	12 x 5 x 2	5 x 4 x 2	2 x 404.6 m + + 110 x 32.9 m + + 10 x 58.7 m + + 16 x 43.8 m
Total arc/wiggler cell length	38.9 m – most of (58.8 m x 10 times)	6.3 m (5 wigglers in row)	1775 m
Dipole/wiggler length (pole face – pole face)	6 m	2.45 m	—
Dipole field /Wiggler peak field	0.1455 T	1.58 T	—
Dipole bend angle	$2\pi/120$	—	—
Electron beam energy	5 GeV		
Electron beam average current	0.400 A		
Chamber vertical full aperture	50 mm	46 mm	50 mm
Chamber horizontal aperture	50 mm	120 mm	50 mm
Required residual gas pressure after 100 Ahr beam conditioning	< 0.5 ntorr CO	< 2 ntorr CO	< 0.1 ntorr CO
Photon critical energy	2.4 keV	26 keV	2.4 keV after arc or 26 keV after wiggler
Photon flux (maximum)	$2.23 \cdot 10^{18}$ photons/(m·s)	$2.43 \cdot 10^{19}$ photons/(m·s)	From 0 to $2.43 \cdot 10^{19}$ photons/(m·s)

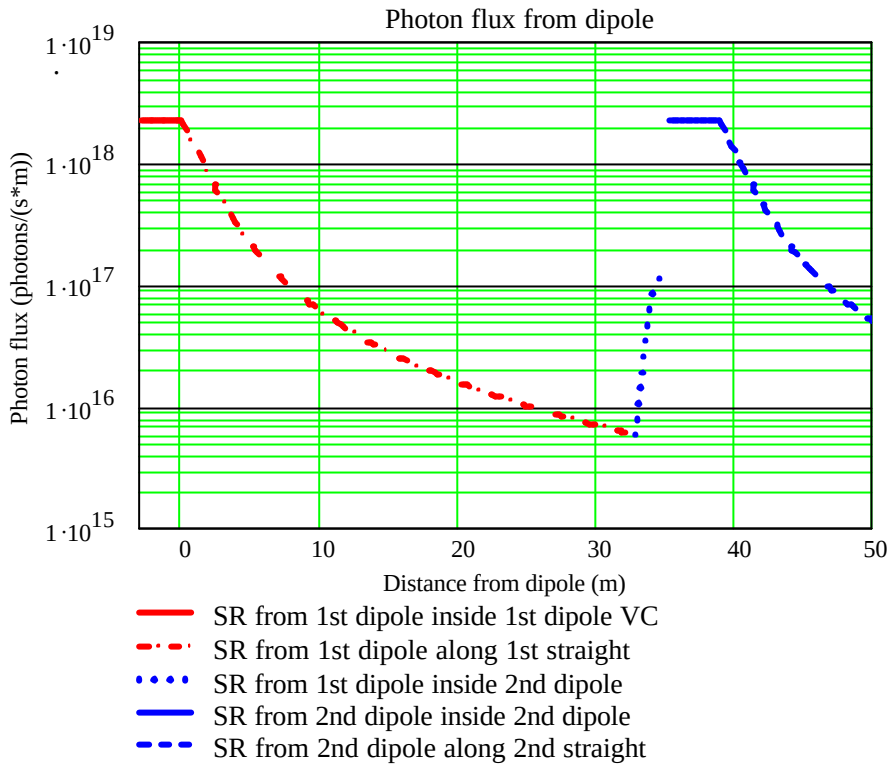

Figure 2. Photon flux onto the vacuum chamber walls inside the dipoles and along the short straights.

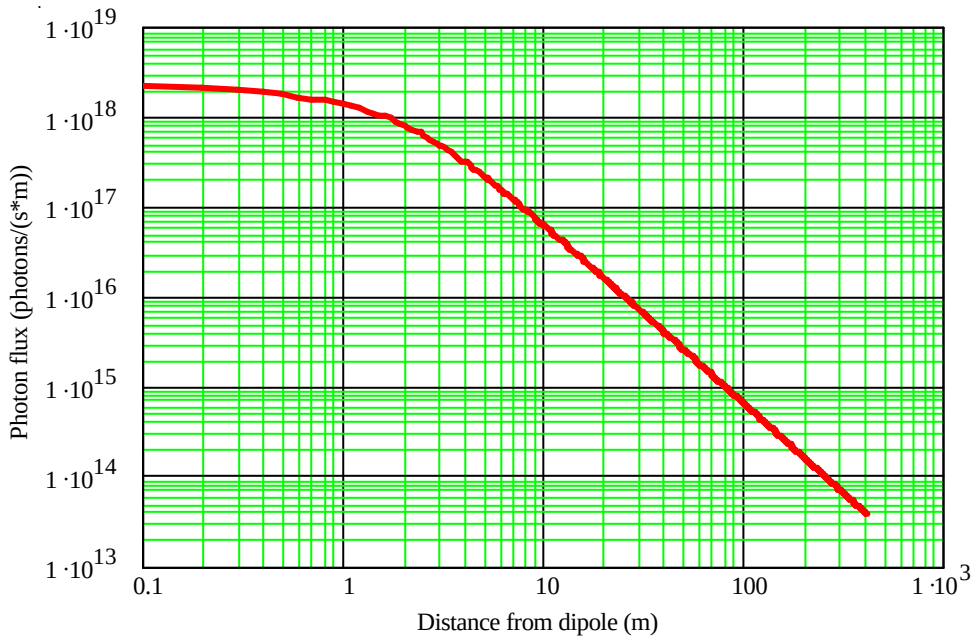

Figure 3. Photon flux onto the vacuum chamber walls as a function of distance from the dipole.

Stainless steel is one of the best conventional materials to use for accelerator vacuum chambers; after bakeout at 300°C for 24 hrs stainless steel provides the lowest photon stimulated desorption. As mentioned above, photodesorption yield reduces with photon dose. Since the photon flux changes along the DR, the photodesorption yield changes as well. Photodesorption yield as a function of distance from a dipole along the damping ring straights is shown in Figure 4 for a stainless steel vacuum chamber baked in-situ at 300°C for 24 hrs. The figures show the photodesorption yield for different amounts of beam conditioning: initial (no conditioning), and after 0.1, 1, 10 and 100 Ahr.

The gas desorption flux q is calculated as a function of the distance from a dipole and the beam conditioning as: $q(z,t) = h\left(D\left(\dot{\Gamma}(z),t\right)\right)\dot{\Gamma}(z)$. The results of desorption flux calculations are also shown in Figure 4. One can see that although the initial desorption flux varies up to 3 decades in the short straights and up to 5 decades in the long straights, the beam conditioning reduces desorption mainly close to the dipole, where photon flux is maximum; as a result, after 100 Ahr the variation in the desorption flux is much reduced: about 10 times in the short straights and 300 times in the long straights (10 times for $0 < z < 50$ m, another 10 times for $50 < z < 200$ m, 3 times for $200 < z < 400$ m).

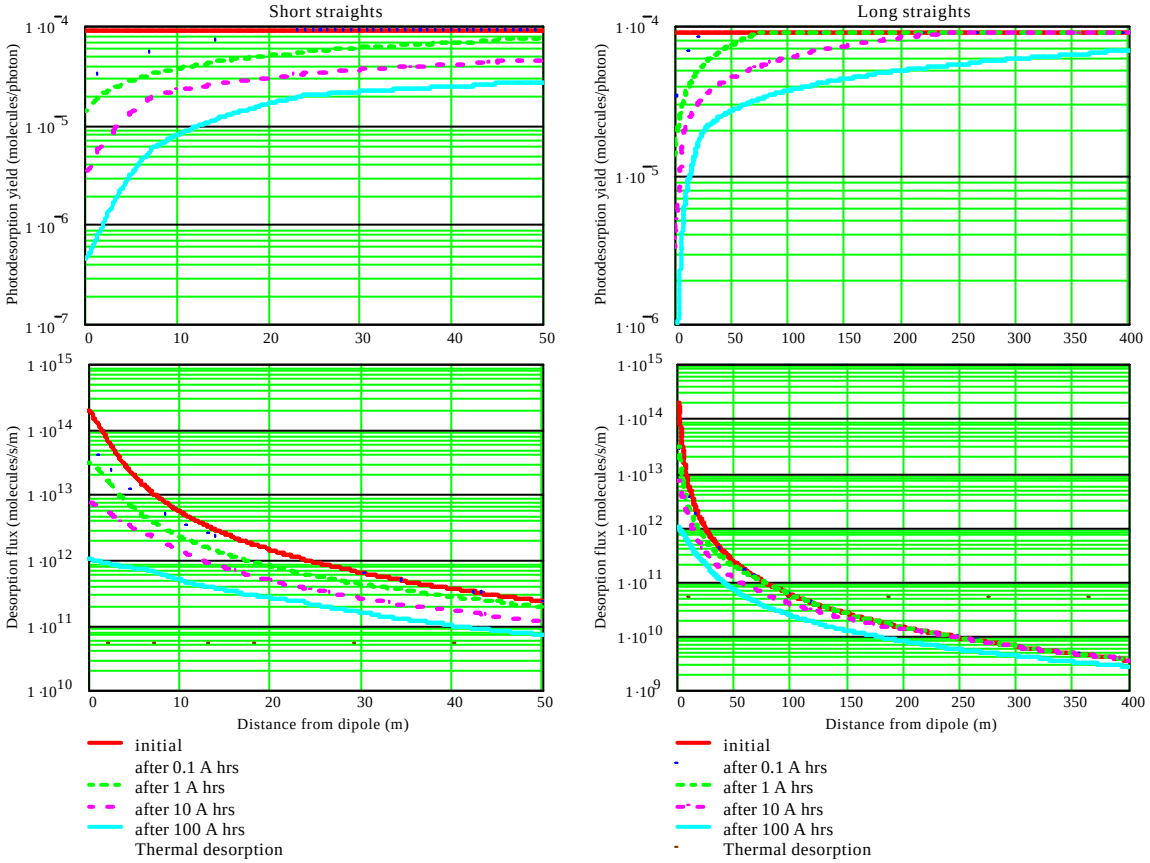

Figure 4. Photodesorption yield and flux as a function of distance from a dipole along the damping ring straights made of stainless steel *tubular vacuum chamber* and baked in-situ at 300°C for 24 hrs. The thermal desorption rate is 10^{-12} Torr×l/(s×cm^2).

The same analysis can be performed for other materials.

Thermal stimulated desorption must also be considered. After bakeout and long pumping the thermal outgassing rate can be in the range of 10^{-12} Torr·l/(s·cm^2) at room temperature. The corresponding thermal desorption in a 50 mm diameter vacuum chamber is shown in Figure 4. One can see that the photon stimulated desorption is the main source of gas in the first 70 m downstream from a dipole; the thermal and photon stimulated desorption are comparable between 70 and 100 m downstream from a dipole; and for distances lager than 100 m the thermal stimulated desorption is larger.

Ante-chamber design

It is widely believed that use of an ante-chamber increases vacuum conductance and allows the reduction of outgassing by localising outgassing at a lumped SR absorber.

The vacuum conductance in a vacuum chamber with an ante-chamber definitely increases. But the wall area increases as well, followed by increased thermal outgassing. If the damping ring vacuum chamber includes a right-angular ante-chamber with dimensions 30 cm x 40 cm the thermal desorption will increase 10 times. Let us first compare the outgassing effects.

Photon stimulated desorption will happen in a few places:

- The SR absorber where photon stimulated desorption will initially be very high, but the absorber will be conditioned very efficiently.
- The vacuum chamber around the SR absorber due to reflected photons and photoelectrons, which escape from the SR absorber. This desorption can be dramatically reduced but not fully suppressed by an intelligent design of the absorber.
- Inside the beam vacuum chamber. This happens because of the small fraction of photons (~5–10% depending on vacuum chamber geometry and beam parameters) that do not enter the antechamber and hit the walls of beam vacuum chamber.

Assuming that 90% of photons are absorbed by SR absorbers and 10% of photons are distributed along the beam vacuum chamber, a gas load analysis can be performed. The distributed gas desorption due to the latter 10% of photons is shows in Figure 5. After 100 Ahr of beam conditioning the distributed photon stimulated desorption due to 10% of photons (i.e. excluding lumped absorber) is the same for both designs: with and without antechamber. Meanwhile, in addition to photon stimulated desorption from the chamber there is thermal outgassing (10 times larger with an ante-chamber) and photon stimulated desorption from the lumped absorber. Therefore the total outgassing inside the vacuum chamber with an antechamber is larger. We should mention that the thermal outgassing also changes with time: the thermal outgassing of a surface irradiated by photons reduces faster. It is reasonable to assume that for a surface irradiated with photons, the thermal desorption reduces proportionally with photon stimulated desorption. Hence, one can conclude that the thermal outgassing will be reduced much faster in a tubular vacuum chamber conditioned with photons than in a vacuum chamber with an ante-chamber.

Therefore, the ante-chamber design does indeed increase the vacuum conductance, but this does not necessarily help in reducing the outgassing. After 100 Ahr of beam conditioning the total outgassing in a tubular vacuum chamber is the same or lower than that in a vacuum chamber with an antechamber. Since it is more expensive, an ante-chamber design will be studied only if it is necessary to deal with other problems such as beam induced electron multipacting and electron cloud.

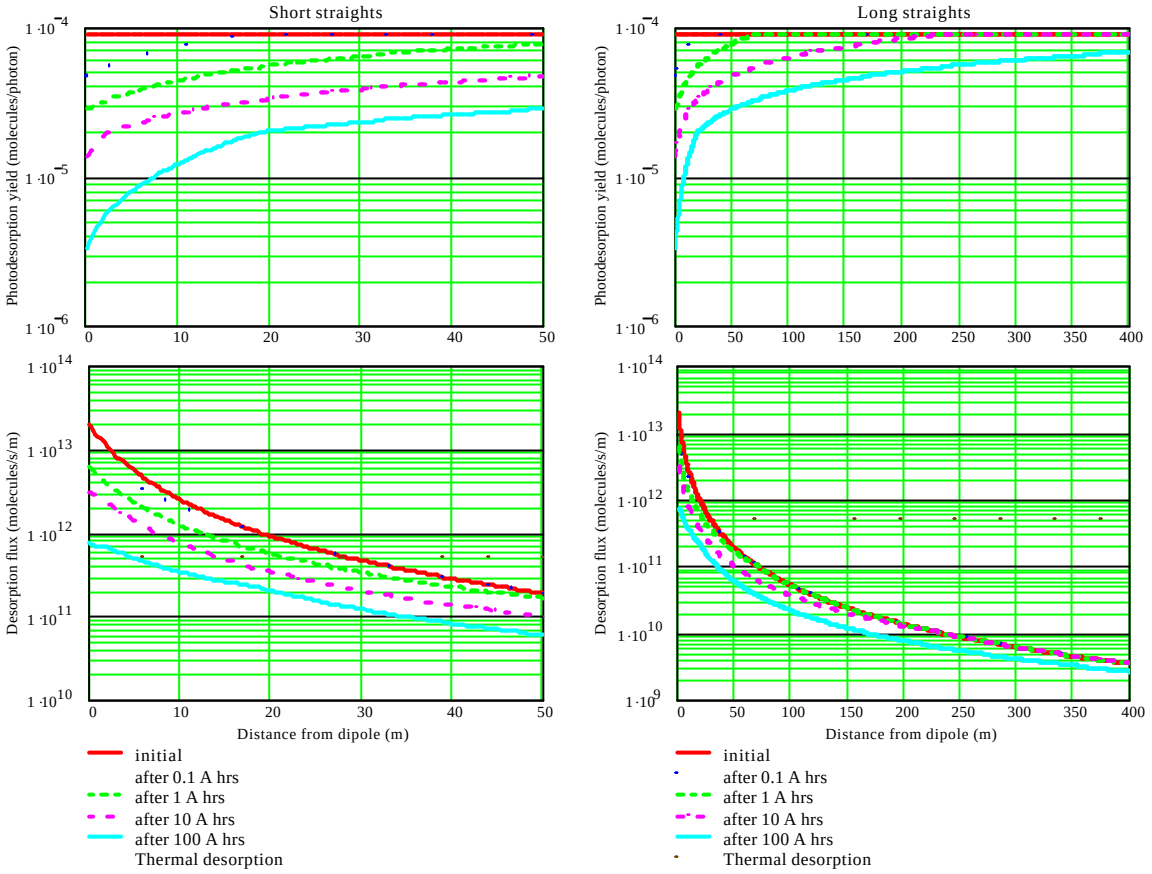

Figure 5. Photodesorption yield and flux as a function of distance from a dipole along a stainless steel vacuum chamber *with an ante-chamber* in the damping ring straights after bake-out in-situ at 300° C for 24 hrs. Thermal desorption rate is 10^{-12} Torr×l/(s×cm^2).

TiZrV NEG coating for accelerator vacuum chambers

A new vacuum technology for accelerators developed at CERN in recent years [9], is the use of TiZrV (NEG) coating for all inner surfaces of the vacuum chamber. TiZrV films have been intensively studied by vacuum groups in many different laboratories [10]. TiZrV coated vacuum chambers are already used in accelerators, for six years at the ESRF [11] and for 4 years at ELETTRA [12]; many others are just beginning (RHIC, Soleil, Diamond) or will use them in future [10]. NEG coating plays a double role: it reduces the outgassing from the vacuum chamber walls (between 10 and 200 times less than *in-situ* baked stainless steel) and it introduces a distributed pumping speed, resulting in lower gas density in a beam vacuum chamber [13]. The only gases which are not pumped by such a coating are hydrocarbons and noble gases; these requires the use of other pumps, (for example, sputter ion pumps) but with much lower pumping speed. The use of NEG coating requires activation, i.e. 24 hours bakeout at 180°C.

It is important to mention that a 1-micron NEG coating can be used on a vacuum chamber made of stainless steel, copper or aluminium.

In a positron DR the NEG coating also plays a role of an anti-multipacting coating.

Thermal stimulated desorption from the NEG is negligible; the pressure inside the NEG coated chamber without SR is less than 10^{-13} Torr (Halmer gauge limit) [14].

4. Gas density calculations for the damping rings

Average pressure (gas density) at room temperature was calculated for the layout shown in Figure 6.

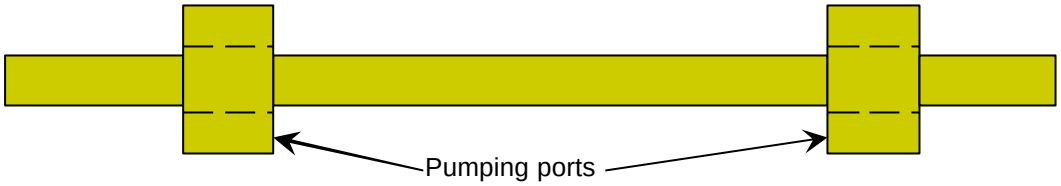

Figure 6. Schematic vacuum chamber layout.

4.1. Pressure along the arc

4.1.1. Pressure inside a stainless steel tube

The pressure was calculated for a stainless steel tube baked *in-situ* to 300°C for 24 hrs and irradiated by photons. The photon stimulated desorption corresponding to 100 Ahr beam conditioning was calculated for four gas species, H_2, CH_4, CO and CO_2, and the thermal desorption for CO with $\eta_t=10^{-12}$ torr·l/(s·cm^2). The average pressure is plotted in Figure 7 as a function of the distance between the vacuum pumps for fixed pumping speed of the pump (on the left hand graph) and as a function of the pumping speed for fixed distance between the vacuum pumps (on the right hand graph). The brown dotted line shows the required pressure in CO equivalent.

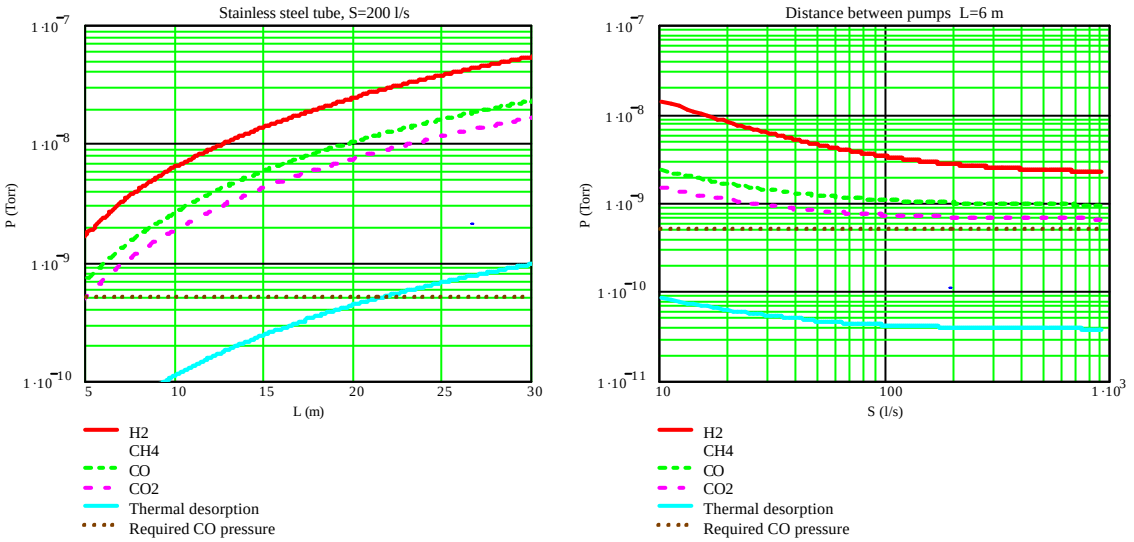

Figure 7. Pressure inside the dipole in a stainless steel vacuum chamber after 100 Ahr beam conditioning as a function of the distance between pumps (left) and as a function of the pumping speed (right).

One can see that the required pressure can be nearly achieved after 100 days beam conditioning for the stainless steel vacuum chamber with a vacuum pump of 200 l/s every 5

metres. It is necessary to consider here that the dipole length is 6 m. The average pressure can not be reduced by increasing the pumping speed because it is limited by the vacuum conductance. The reduction of the distance between the pumps or introduction of an antechamber for better conductance leads to a more expensive design and increases the thermal outgassing level dramatically; therefore it is not optimum.

4.1.2. Pressure inside a NEG coated tube

Results of pressure calculations for a similar vacuum chamber with NEG coating of the entire surface of the vacuum chamber are shown in Figure 8. As described above, the NEG coating dramatically reduces outgassing and introduces distributed pumping. The pressure just after activation is almost the same as in the stainless steel vacuum chamber after 100 Ahr conditioning, but the required pumping speed of lumped pumps is just 20 l/s every 5 m. After 100 Ahr conditioning the required pressure can be reached with a much smaller number of pumps: one 20-l/s pump every 30 m. The residual gas spectrum is dominated by methane.

The above calculations were made for a photodesorption flux corresponding to the region inside a dipole. An arc cell consists of a 6 m dipole and a following straight between 33 m and 40 m in length. As shown in Figure 4 the photodesorption flux in the short straight between two dipoles reduces 10 times after 100 Ahr conditioning, therefore the average pressure along all sections will be a few times less. The practical solution in this case is one 20 l/s sputter ion pump per arc cell installed immediately downstream of the dipole.

4.2. Pressure along the wiggler section

4.2.1. Pressure inside a copper tube

The wiggler vacuum chamber should absorb significant SR power, therefore is quite likely that it will be made of copper. Results of pressure calculations are shown in Figure 9. One can see that the required pressure can be achieved after 100 days beam conditioning for the copper vacuum chamber with a vacuum pump of 200 l/s every 3 metres. It is necessary to consider here that the wiggler cell length is 6.3 m; i.e. to meet the vacuum requirements it is necessary to apply either distributed pumps or an antechamber design to let SR out of the wiggler, and to absorb the SR power with a lumped absorber (~100 kW per 6.3 m wiggler cell).

Initial

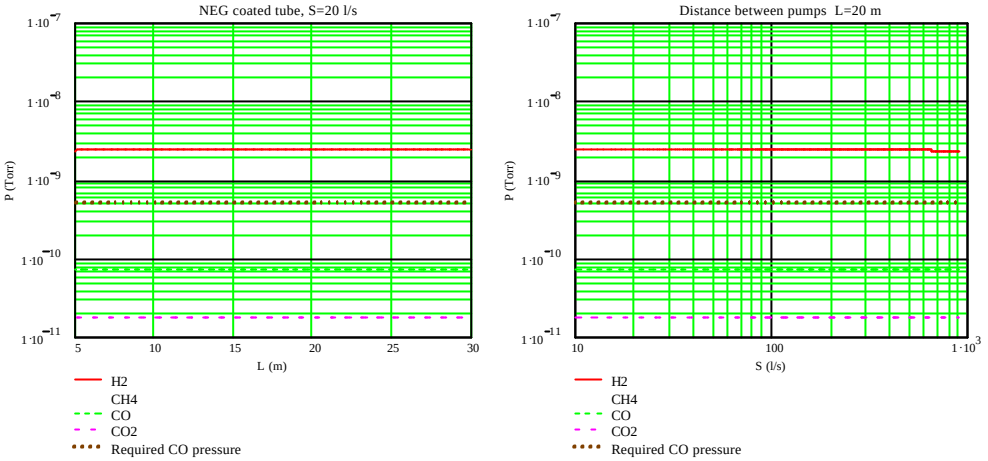

After 100 Ahr beam conditioning

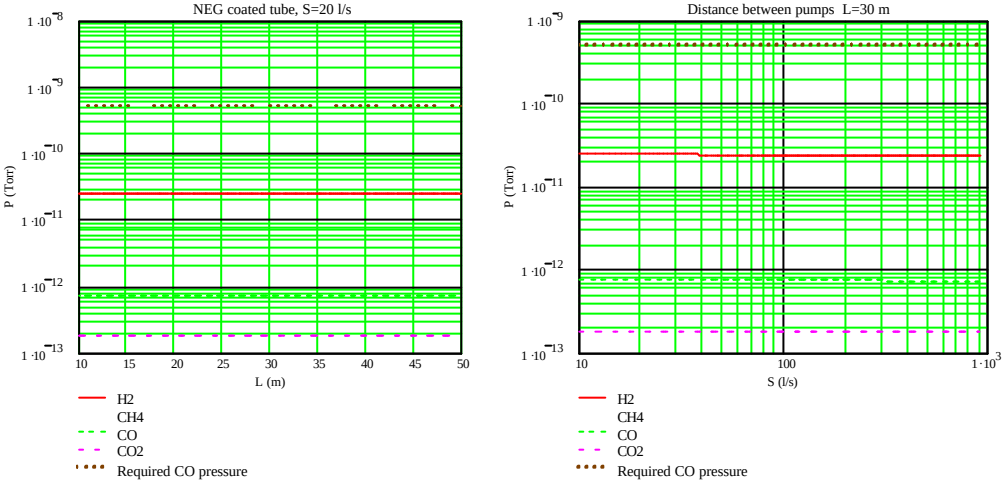

Figure 8. Pressure inside the dipole in a NEG coated vacuum chamber, initially and after 100 Ahr beam conditioning, as a function of the distance between pumps (left) and as a function of the pumping speed (right).

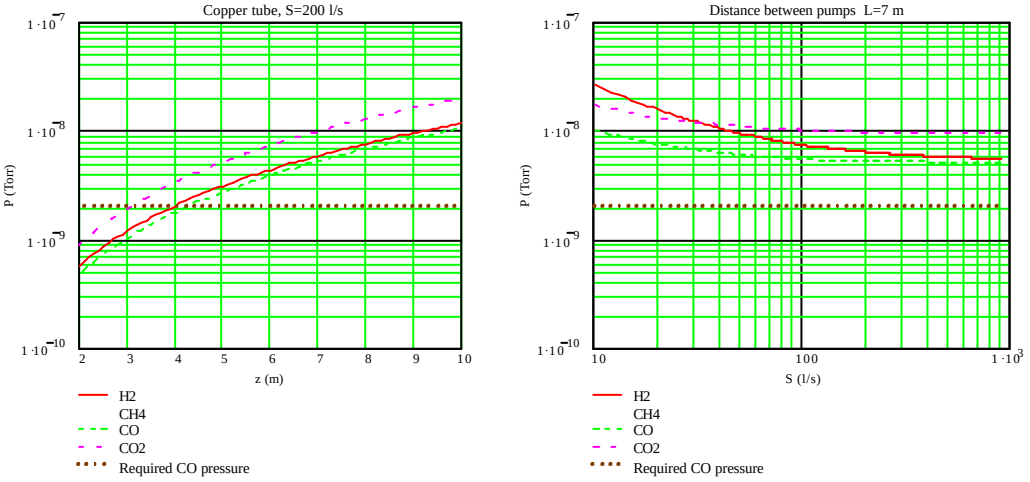

Figure 9. Pressure inside a wiggler copper vacuum chamber after 100 Ahr beam conditioning, as a function of the distance between pumps (left) and as a function of the pumping speed (right).

4.2.2. Pressure inside a NEG coated wiggler vacuum chamber

Use of NEG coating also helps inside the wiggler vacuum chamber. The initial pressure is 10 times larger than the required pressure, but after 100 Ahr conditioning the required pressure is reached with one 20-l/s pump every 12 m. The residual gas spectrum is dominated by methane.

In the damping rings, five wigglers will be located sequentially; 20 l/s sputter ion pumps could be installed before/after each wiggler (six pumps for five wigglers).

An ante-chamber design may be required to deal with the SR power generated by the wigglers (~16 kW/m) and to suppress electron multipacting in the positron DR. In this case, use of NEG coating is recommended for both the beam chamber and the antechamber to reduce thermal and photon stimulated desorption and to reduce secondary electron emission.

Initial

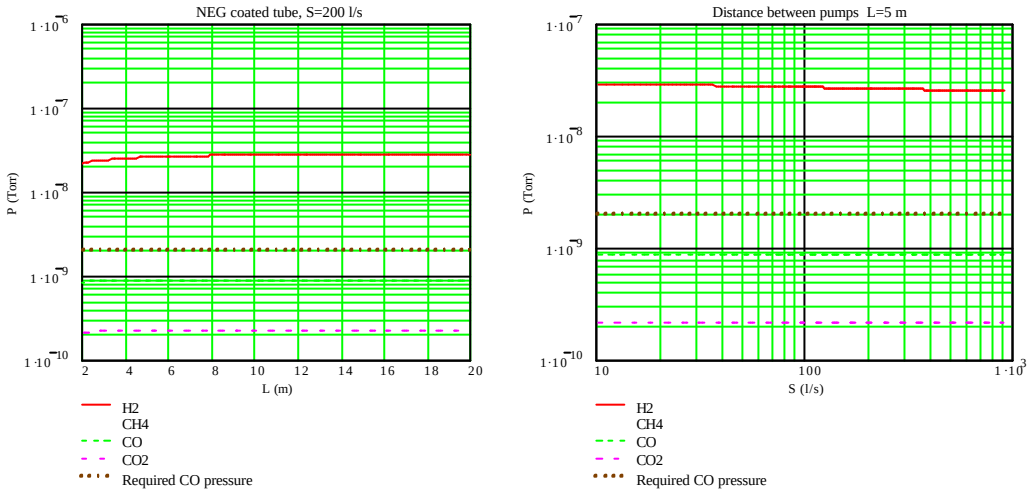

After 100 Ahr beam conditioning

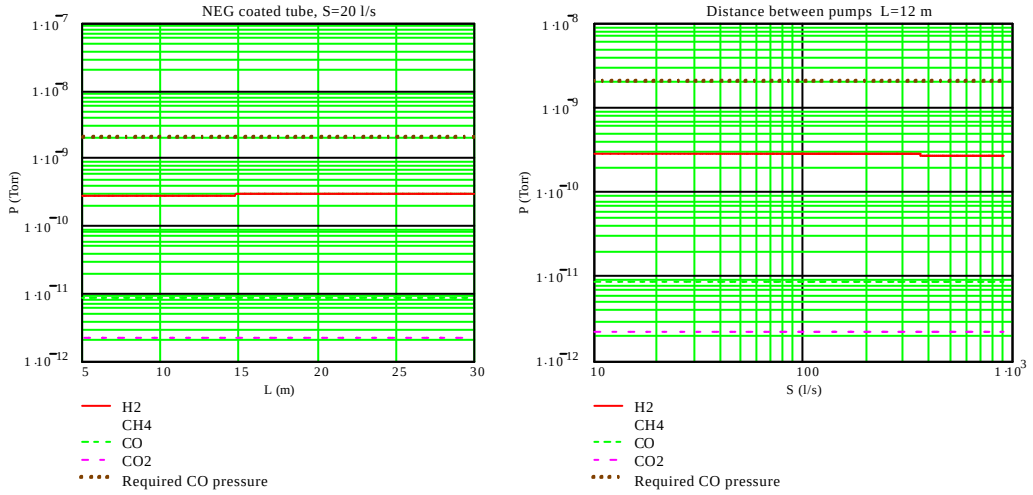

Figure 10. Pressure inside the dipole in a NEG coated wiggler vacuum chamber, initially and after 100 Ahr beam conditioning, as a function of the distance between pumps (left) and as a function of the pumping speed (right).

4.3. Pressure along the Long Straight sections

The long straight sections will be irradiated by the SR from a dipole. The first 50 m from a dipole are the same as in an arc cell but the required vacuum is much higher – 10^{-10} Torr. There are two possible solutions:

- First, one may use NEG coating everywhere: since NEG coating works where the SR is very intense (arcs and wigglers) it will also work where SR is less intense.
- Second, one may use stainless steel with conventional vacuum technology (bakeout and pumps) where SR is less intense.

As mentioned above, the SR induced gas desorption is about 10 times less at z= 40 m, ~100 times less at 170 m, and ~300 times less at z = 350 m. The results of calculations for a stainless steel coated vacuum chamber are shown in Figure 11 for z = 40 m and Figure 12 for z = 170. In this case, 100 l/s pumps are required every 6 m for 40 < z < 120 m, every 10 m for 80 < z < 400 m, and every 40 m for 160 < z < 400 m.
The results of calculations for a NEG coated vacuum chamber are shown in Figure 13 for z = 40 m and Figure 14 for z = 170 m. One can see that with NEG coating, 20 l/s pumps are required every 10 m for 0 < z < 80 m, every 20 m for 80 < z < 160 m, and every 40 m for 160 < z < 400 m.

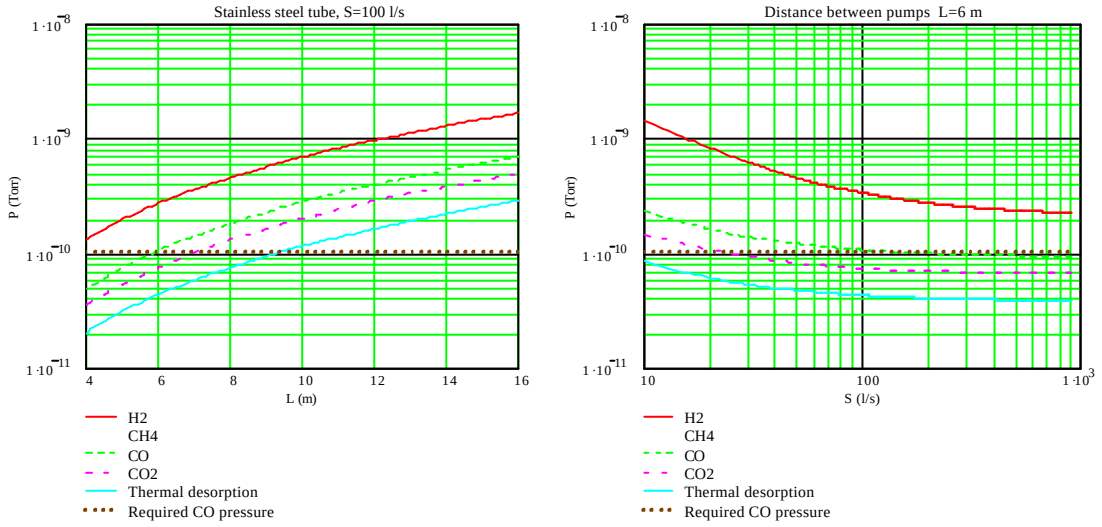

Figure 11. Pressure inside the dipole in a stainless steel Long Straight Section vacuum chamber after 100 Ahr beam conditioning, 40 m downstream from a dipole, as a function of the distance between pumps (left) and as a function of the pumping speed (right).

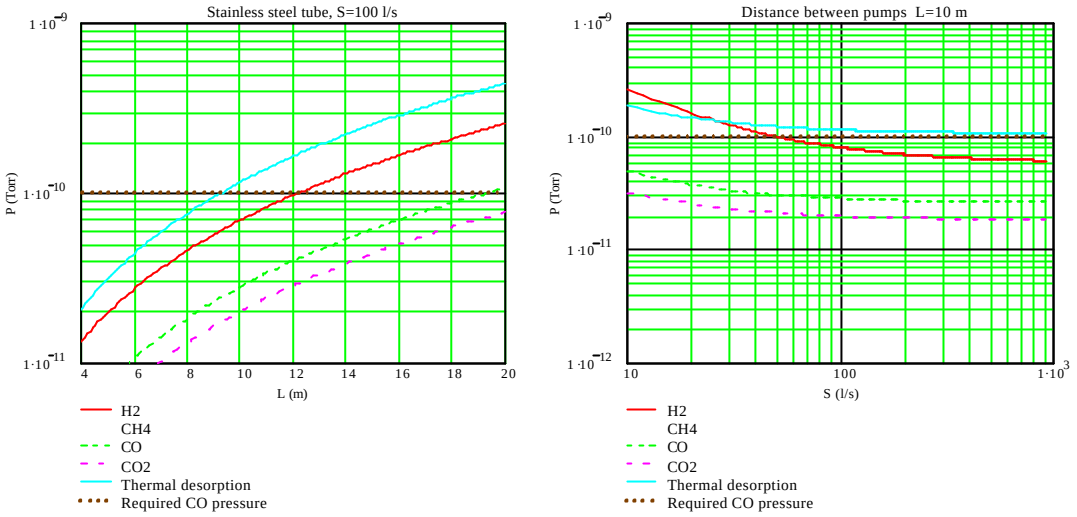

Figure 12. Pressure inside the dipole in a stainless steel Long Straight Section vacuum chamber after 100 Ahr beam conditioning, 170 m downstream from a dipole, as a function of the distance between pumps (left) and as a function of the pumping speed (right).

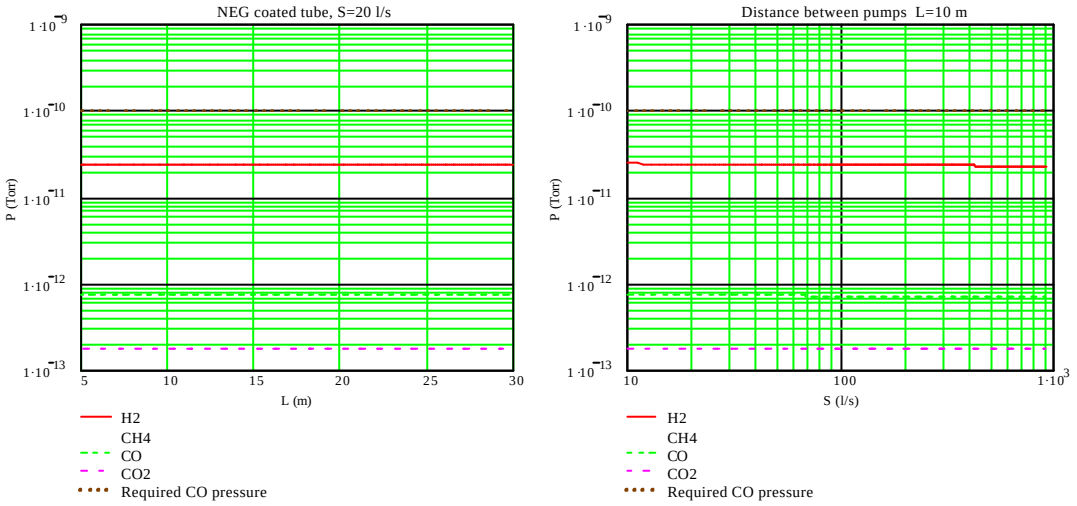

Figure 13. Pressure inside the dipole in a NEG coated Long Straight Section vacuum chamber for 0-100 m downstream from a dipole, after 100 Ahr beam conditioning, as a function of the distance between pumps (left) and as a function of the pumping speed (right).

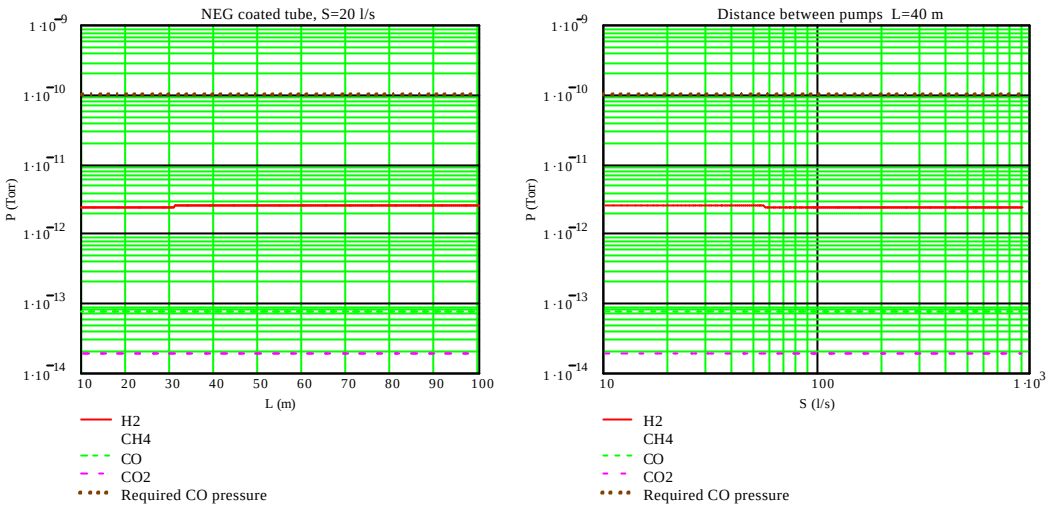

Figure 14. Pressure inside the dipole in a NEG coated Long Straight Section vacuum chamber 170 m downstream from a dipole, after 100 Ahr beam conditioning, as a function of the distance between pumps (left) and as a function of the pumping speed (right).

5. Conclusions

NEG coating of the entire vacuum chamber appears to be the cheapest solution for the ILC damping rings, since the vacuum system will then require fewer pumps with lower pumping speed. In this case, the pumps that will be required are as follows:

- Each of the 120 arc cells will require one 20-l/s sputter ion pump installed immediately downstream of the dipole.
- Each of the eight wiggler sections of 5 wigglers located sequentially will require six 20-l/s sputter ion pumps. The first pump should be installed in front of the first wiggler, then one additional pump between each pair of wigglers, and finally one further pump after last wiggler.
- In the long straight sections, 20-l/s pumps will be required every 10 m for $0 < z < 80$ m, every 20 m for $80 < z < 160$ m, and every 40 m for $160 < z < 400$ m.

Acknowledgments

This work is supported by the Commission of the European Communities under the 6th Framework Programme “Structuring the European Research Area”, contract number RIDS-011899.

References

[1] Configuration Studies and Recommendations for the ILC Damping Rings. Edited by A.Wolski et al., LBNL-59449, Lawrence Berkeley National Laboratory, Berkeley, CA 94720, USA. February 4, 2006.
[2] Lanfa Wang, private communication.
[3] C. Herbeaux, P. Martin, V. Baglin and O. Gröbner. "Photon stimulated desorption of an unbaked stainless steel chamber by 3.75 keV critical energy photons." J.Vac.Sci.Technol A17(2), Mar/Apr 1999, pp.635–643.
[4] C.L. Foerster, H. Halama and C. Lanni. "Photon-stimulated desorption yields from stainless steel and copper-plated beam tubes with various pre-treatments." J.Vac.Sci.Technol A8(3), May/June 1990, pp.2856–2859.
[5] O. Gröbner, A.G. Mathewson and P. Martin. "Gas desorption from an oxygen free high conduvctivity copper vacuum chamber by synchrotron radiation photons." J.Vac.Sci.Technol A12(3), May/Jun 1994, pp.846–853.
[6] J. Gomez-Goni, O. Gröbner and A.G. Mathewson. Comparison of photodesorption yields using synchrotron radiation of low critical energies for stainless steel, copper and electro-polished copper surfaces. J.Vac.Sci.Technol. A 12(4), pp. 1714–1718, Jul/Aug 1994.
[7] J.C. Billy, J.P. Bojon, B Henrist, N. Hilleret, M.J. Jimrnrz, I. Laugier, P. Stubin. The pressure and gas composition evolution during the operation of the LEP accelerator at 100 GeV. Vacuum 60, 2001, pp. 183-189.
[8] V.V. Anashin, O.B. Malyshev, V.N. Osipov, I.L. Maslennikov and W.C. Turner. “Investigation of synchrotron radiation-induced photodesorption in cryosorbing quasi-closed geometry”, J.Vac.Sci.Technol. A 12(5), pp. 2917–2921, Sep/Oct 1994.
[9] C. Benvenuti. Non-Evaporable Getters : from Pumping Strips to Thin Film Coatings. EPAC '98 , Stockholm, Sweden , 22 - 26 Jun 1998, pp. 200-204.
[10] 45th IUVSTA Workshop on NEF coatings for particle accelerators and vacuum systems. 5-8 April 2006. Catania, Italy. *www.iuvsta.org.*
[11] M. Hahn and R. Kersevan. Status of NEFG coating at ESRF. Proc. of 2005 Particle Accelerator Conference, Knoxville, Tennessee, pp. 422-424.
[12] F. Mazzolini, L. Rumiz, J. Miertusova, F. Pradal. Ten years of ELETTRA vacuum system experience. Vacuum 73 (2004) 225–229.
[13] V.V. Anashin, I.R. Collins, R.V. Dostovalov, N.V. Fedorov, A.A. Krasnov, O.B. Malyshev and V.L. Ruzinov. Comparative study of photodesorption from TiZrV coated and uncoated stainless steel vacuum chambers. Vacuum 75 (2), July 2004, pp. 155-159.
[14] C. Benvenuti et al. A novel route to extreme vacua: the non-evaporable getter thin film coatings. Vacuum 53 (1999) 219–225.